

© 2016. This manuscript version is made available under the CC-BY-NC-ND 4.0 license  
<http://creativecommons.org/licenses/by-nc-nd/4.0/>

<https://doi.org/10.1016/j.solmat.2016.09.023>

# CdS and $Zn_{1-x}Sn_xO_y$ buffer layers for CIGS solar cells

P.M.P Salomé<sup>1,#</sup>, J. Keller<sup>2</sup>, T. Törndahl<sup>2</sup>, J.P. Teixeira<sup>3</sup>, N. Nicoara<sup>1</sup>, R-Ribeiro Andrade<sup>1,4</sup>, D. G. Stroppa<sup>1</sup>, J. C. González<sup>4</sup>, M. Edoff<sup>2</sup>, J.P. Leitão<sup>3</sup>, S. Sadewasser<sup>1</sup>

<sup>1</sup> International Iberian Nanotechnology Laboratory, 4715-330 Braga, Portugal

<sup>2</sup> Ångström Laboratory, Solid State Electronics, Ångström Solar Center, Uppsala University, SE-751 21 Uppsala, Sweden

<sup>3</sup> Departamento de Física and I3N, Universidade de Aveiro, 3810-193 Aveiro, Portugal

<sup>4</sup> Departamento de Física, Instituto de Ciências Exatas, Universidade Federal de Minas Gerais, Caixa Postal 702, 30123-970 Belo Horizonte, MG, Brasil

# [pedro.salome@inl.int](mailto:pedro.salome@inl.int)

## Abstract

Thin film solar cells based on  $Cu(In,Ga)Se_2$  (CIGS), where just the buffer layer is changed, were fabricated and studied. The effects of two different buffer layers, CdS and  $Zn_xSn_{1-x}O_y$  (ZnSnO), are compared using several characterization techniques. We compared both devices and observe that the ZnSnO-based solar cells have similar values of power conversion efficiency as compared to the cells with CdS buffer layers. The ZnSnO-based devices have higher values in the short-circuit current ( $J_{sc}$ ) that compensate for lower values in fill factor (FF) and open circuit voltage ( $V_{oc}$ ) than CdS based devices. Kelvin probe force microscopy (KPFM) results indicate that CdS provides junctions with slightly higher surface photovoltage (SPV) than ZnSnO, thus explaining the lower  $V_{oc}$  potential for the ZnSnO sample. The TEM analysis shows a poly-crystalline ZnSnO layer and we have not detected any strong evidence of diffusion of Zn or Sn into the CIGS. From the photoluminescence measurements, we concluded that both samples are being affected by fluctuating potentials, although this effect is higher for the CdS sample.

**Keywords:** thin film solar cells;  $Cu(In,Ga)Se_2$  (CIGS); buffer layers; CdS;  $Zn_{1-x}Sn_xO_y$

## 1 Introduction

Thin film solar cells based on  $Cu(In,Ga)Se_2$  (CIGS) have recently achieved a certified power conversion efficiency of 22.8 % [1], which is a significant increase from the 2013 value of 20.4 % [2]. This recent improvement was achieved by the development of a new process on the CIGS surface consisting of evaporating KF after the growth of the CIGS layer and prior to the deposition of the buffer layer. Its full effects are still being studied but it has been shown that this process creates a CIGS/buffer junction with better properties by increasing the solar cell open circuit voltage,  $V_{oc}$ , and fill factor, FF [3]. The highest performance CIGS solar cells were achieved with a buffer layer consisting of CdS deposited by chemical bath deposition (CBD). However, CdS as a buffer layer exhibits some intrinsic problems: i) low bandgap energy,  $\sim 2.4$  eV, that prevents high energy photons from arriving to the CIGS; ii) it contains the toxic element Cd; and iii) it is deposited with a non-vacuum method which is not favourable since the processes that are made before and after the buffer layer deposition are vacuum-based [4]. The ideal buffer layer

should have: i) electrical properties as good as the ones of CdS, if not better; ii) a higher bandgap energy than the one of CdS; iii) contain only non-toxic elements; and iv) allow deposition by a vacuum compatible technique. Many Cd-free materials have been proposed and studied [4]. However, the resulting solar cells usually lag behind CdS solar cells in terms of  $V_{oc}$  and FF; for example, the previous world record solar cells achieved a value of 21.7 % with CdS but only 21 % with Zn(S,O) [5]. Solar cells with Cd-free buffer layers usually achieve higher values of short circuit current,  $J_{sc}$ , due to their higher band gap energy compared with CdS. In this paper we focus on the alternative buffer material  $Zn_{1-x}Sn_xO_y$  (ZnSnO). Solar cell devices with a ZnSnO buffer layer have achieved values of power conversion efficiency above 18 % and performing on the same efficiency level as CdS [6-8]. These results are quite promising, nevertheless further studies are needed for a better understanding of this material and to identify if it imposes the same benefits to the CIGS as CdS buffer layers.

In view of the recently shown importance of the front interface and the general search for Cd-free buffer layers, in this work, we performed a comparison between CIGS devices prepared with CdS and with ZnSnO buffer layers. Several techniques were used to assess the differences between the electrical behaviour of devices with CdS or with ZnSnO buffer layers. We would like to emphasize that in this study we used CIGS grown using an in-line and semi-industrial pilot tool evaporator. These processes are very similar to industrial ones: a) the substrates are glasses without diffusion barriers [9]; b) the Mo layer is thin to cut costs and deposited in a batch reactor with no control over its oxidation [10]; c) the CIGS was grown in a batch reactor on large substrates (12.5x12.5 cm) [8]; d) the TCO layers are thick; and e) no anti-reflective (AR) coatings are used.

## 2 Experimental

### 2.1 Materials preparation

Solar cells with the structure soda-lime glass(SLG)/Mo/CIGS/buffer/i-ZnO/ZnO:Al/Ni-Al-Ni-grid without AR coating were prepared at Uppsala University using the Ångström solar cell baseline [8]. CIGS was prepared in an in-line evaporator using a one stage co-evaporation process [8]. The positioning of the sources resulted in a linearly decreasing  $[Ga]/([Ga]+[In])$  ratio from the back contact to the front of the film [11] and a detailed characterization of this type of profile can be found elsewhere [11]. The tool co-evaporates CIGS on 12.5x12.5 cm<sup>2</sup> substrates. The composition of the CIGS used in this study was  $[Ga]/([In]+[Ga]) = 0.42 \pm 0.03$  and  $[Cu]/([In]+[Ga]) = 0.86 \pm 0.03$ . The thickness was measured to be  $1.85 \pm 0.25 \mu m$ , using a Panalytical Epsilon 5 X-ray fluorescence (XRF) system with a CIGS calibration sample. In addition, elemental depth profiles of the CIGS layer were recorded with glow discharge optical emission spectroscopy (GDOES) in a Spectrumba GDA750 (Spectrumba Analytik GmbH, Germany) [12]. The composition and thickness values of the GDOES measurements were integrated/corrected using the XRF values. A single substrate was split so that part was covered with CdS, whereas another part was covered with ZnSnO, thus our devices are based on the same CIGS. Additionally, this step ensures that both the handling of the glass substrate prior to deposition and the Mo layer are the same for the compared devices. After the buffer deposition the same solar cell processing was done on both samples consisting of sputtering of i-ZnO and ZnO:Al, e-beam evaporation of Ni/Al/Ni grids, and scribing. In that way 12 solar cells were fabricated for each buffer layer. For the characterizations that needed non-finished solar cells, i.e. SLG/Mo/CIGS/buffer, additional pieces of the sample were used where the processing finished right after the deposition, as shown in figure 1. To prevent any possible degradation of the materials, storage, transport, and shipping of all samples, were made either in low-vacuum, or in a dry N<sub>2</sub> environment.

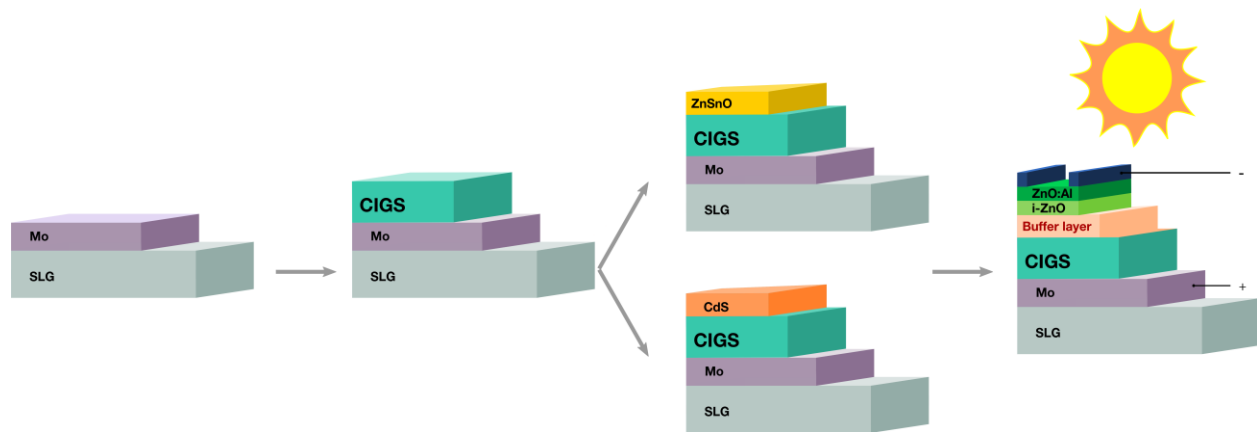


Figure 1: Representation of the fabrication and design of experiment. In the process of fabricating of the solar cell, the only step where the devices were not processed at the same time was the buffer layer deposition.

CdS was deposited by conventional CBD with a solution of 1.1 M ammonia, 0.100 M thiourea, and 0.003 M cadmium acetate. The solution is mixed in a beaker at room temperature, and the samples are immersed into the beaker, which is subsequently heated to 60 °C in a water bath. During the growth process, the solution is stirred for 10 s each minute. The baseline process time is 8 min and 15 s, and the samples are then directly removed from the CBD beaker and immersed in clean deionized water to stop the growth process. This process typically produces films with a thickness of 50-70 nm. For the photoluminescence measurements, CdS was etched using a 5% HCl solution during 30 s. The estimated time interval between the etching and the mounting of the sample in the cryostat, in helium atmosphere, was minimized, circa 5 mins, in order to avoid the degradation of the CIGS layer [13, 14].

The ZnSnO buffer layer was grown by using a Microchemistry F-120 ALD reactor kept at a deposition temperature of 120 °C according to a previously developed process [6]. As precursors, diethyl zinc (DEZn or  $\text{Zn}(\text{C}_2\text{H}_5)_2$ ), tetrakis (dimethylamino) tin (TDMASn or  $\text{Sn}(\text{N}(\text{CH}_3)_2)_4$ ), and deionized water ( $\text{H}_2\text{O}$ ) were used together with nitrogen gas ( $\text{N}_2$ ) as carrier and purge gas. A total of 625 ALD cycles were deposited, where the pulse lengths were 400/400:800:400:800 ms long for the Sn/Zn precursor: $\text{N}_2$ : $\text{H}_2\text{O}$ : $\text{N}_2$  pulses, respectively. The  $[\text{Sn}]/([\text{Sn}]+[\text{Zn}])$  pulse ratio was set to 0.4 in order to produce a buffer layer with an x-value of around 0.2.

## 2.2 Characterization techniques

Completed solar cell devices were characterized by current density-voltage (J-V) measurements with illumination from an ELH lamp. Values of FF,  $J_{sc}$ ,  $V_{OC}$ , and power conversion efficiency were extracted from the J-V curves as well as other parameters as explained elsewhere [15]. The shown values are averages of 12 cells together with its standard deviation. External quantum efficiency (EQE) was determined under ambient light, using chopped monochromatic light that was scanned through the wavelength interval of 360–1200 nm in 2-nm steps. To obtain the capacitance-voltage, C-V, characteristics, an Agilent 4294A impedance analyser with a DC voltage sweep range between -1.0 V to +0.6 V using 0.1 V steps and a frequency of 10 kHz with an AC modulation voltage of 50 mV rms was used. These measurements were performed at room temperature and in dark conditions. After the sample preparation and electrical characterization the samples were transferred to INL for further investigations.

Scanning transmission electron microscopy (STEM) images were taken with a FEI Titan Themis 80-300 kV Cs-probe corrected transmission electron microscope, operating at 300 kV accelerating potential and equipped with an EDS-Bruker silicon drift detector. In this method a coherent focused probe scans across the specimen and the X-ray emission spectrum is recorded in each probe position. Conventional high resolution transmission electron microscope (HRTEM) images were taken with a Jeol JEM 2100 80-200 kV operating at 200 kV. The lamellas were prepared in a focused ion beam (FIB) FEI Dual-Beam Helios 450S with FIB Cu-grids using a technique known as "lift-out" [16]. On top of the buffer layer we deposited a protective Pt bi-layer using the electron beam and the Ga beam. The ZnSnO lamella was ion milled to a high extent and thus the second Pt layer is not seen, such detail does not cause differences in the interpretation of the results shown here. Despite using the Ga ion beam with low energy (2 KeV) in the final polishing to remove amorphous Ga, this layer is significantly reduced. However we cannot say that this layer is completely removed on the samples and therefore the Ga counts from the EDS analysis are not reliable.

Kelvin probe force microscopy (KPFM) experiments were performed in an ultra-high vacuum (UHV) scanning probe microscope (SPM), Omicron Nanotechnology GmbH, controlled by Nanonis electronics and using a PtIr-coated cantilever ( $f_0 = 169$  kHz). The amplitude modulation technique was used for the detection of the contact potential difference (CPD) with an ac bias of 200 mV at the second oscillation mode of the cantilever. CPD is defined as the difference in work function ( $\Phi$ ) between the sample and the tip:  $CPD = \Phi_{\text{sample}} - \Phi_{\text{tip}}$ . The same tip was used for all reported measurements to ensure comparability of the CPD values between the measurements and between the two samples (CIGS/CdS and CIGS/ZnSnO). To determine the surface photovoltage (SPV), the CPD was measured with the sample illuminated by a red laser, 635 nm, and optical power of 4.5 mW, under an illumination angle of  $28^\circ$ , to ensure illumination of the sample under the tip and cantilever beam. From a pair of CPD images in the dark and under illumination, the SPV is calculated according to  $SPV = CPD_{\text{light}} - CPD_{\text{dark}}$  [17]. For the average values given in Table 2 several image pairs (dark and illuminated) taken in different regions of each sample were analysed.

The photoluminescence (PL) measurements were carried out using a Bruker IFS 66v Fourier Transform Infrared (FTIR) spectrometer equipped with a Ge-diode detector. The samples were inserted in a helium gas flow cryostat which allows for measurements at 5 K. The excitation source was the 514.5 nm line of an Ar<sup>+</sup> ion laser, with the laser power measured at the front of the cryostat window. The PL spectra were corrected for the sensitivity of the Ge detector. The range of excitation power values used for the two samples was different due to the detector saturation at different excitation power values during the measurement of each sample.

### 3 Results

#### 3.1 Crystalline structure and chemical analysis

In figure 2 a GDOES analysis of the CIGS absorber layer is presented. Elemental ratios are corrected with respect to the XRF-determined composition whereas the Na and Mo values are the uncalibrated GDOES counts. The analysis shows a nearly linear  $[Ga]/([Ga]+[In])$  gradient with a value of 0.55 at the back and close to 0.33 at the surface. In comparison with similar measurements made on our most efficient solar cells [18], the overall Ga concentration is higher and the Ga profile is flatter in the present samples. We

also note the typical Na distribution profile that shows an increased concentration at both absorber interfaces compared with the bulk of the absorber and the typical flat  $[Cu]/([Ga]+[In])$ .

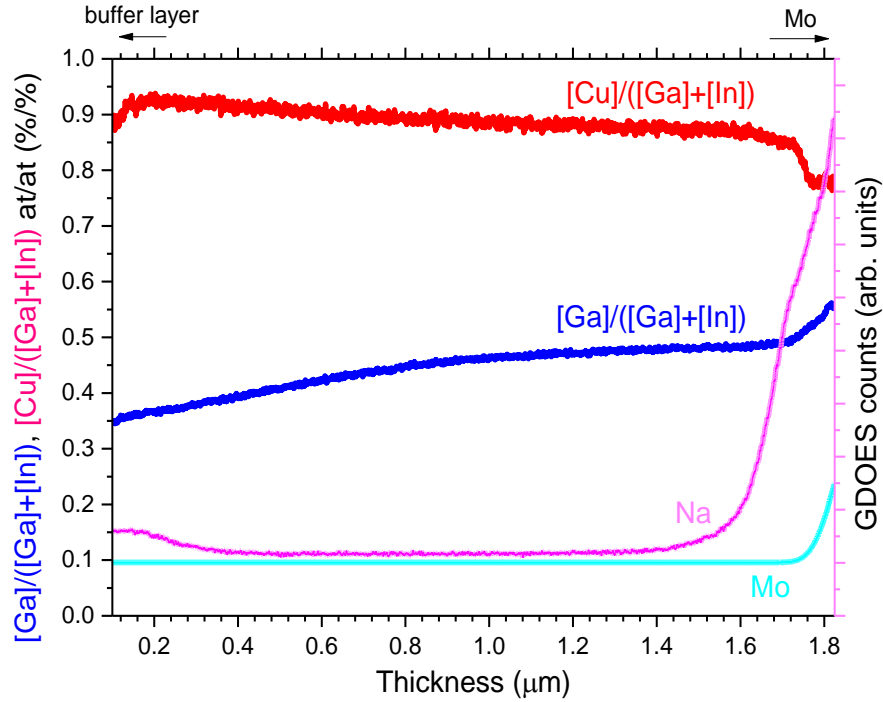


Figure 2: Elemental depth profile of  $[Ga]/([Ga] + [In])$ ,  $[Cu]/([Ga] + [In])$ , and counts of Na and Mo, measured by GDOES for the studied CIGS samples and with an overall  $[Ga]/([Ga] + [In])$  value of 42%. The values of  $[Ga]/([Ga] + [In])$ ,  $[Cu]/([Ga] + [In])$  were calibrated using XRF measurements.

Figure 3 (a) and 3 (b) show the high angular annular dark field (HAADF) images of CdS and ZnSnO layers, respectively. From these images we see that both the CdS and ZnSnO layers are covering the CIGS surface homogeneously. The images also show that both buffer layers do not present pin-holes. This information is more important for the ZnSnO layer, since it is thinner than the CdS layer. We estimated a thickness of  $56 \pm 12$  nm for the CdS layer and  $17 \pm 5$  nm for the ZnSnO layer. These thicknesses are inside the expected values of 50-70 nm for the CdS layer and 20-30 nm for the ZnSnO layer. The Pt layer, which was deposited by assistance of an electron beam, did not adhere homogeneously on either layer. Another important observation revealed by the TEM analysis was the confirmation of the presence of nano-crystalline domains both in the CdS and in the ZnSnO layers. Figure 3 (c) is a conventional HRTEM image that shows ZnSnO nano-domains.

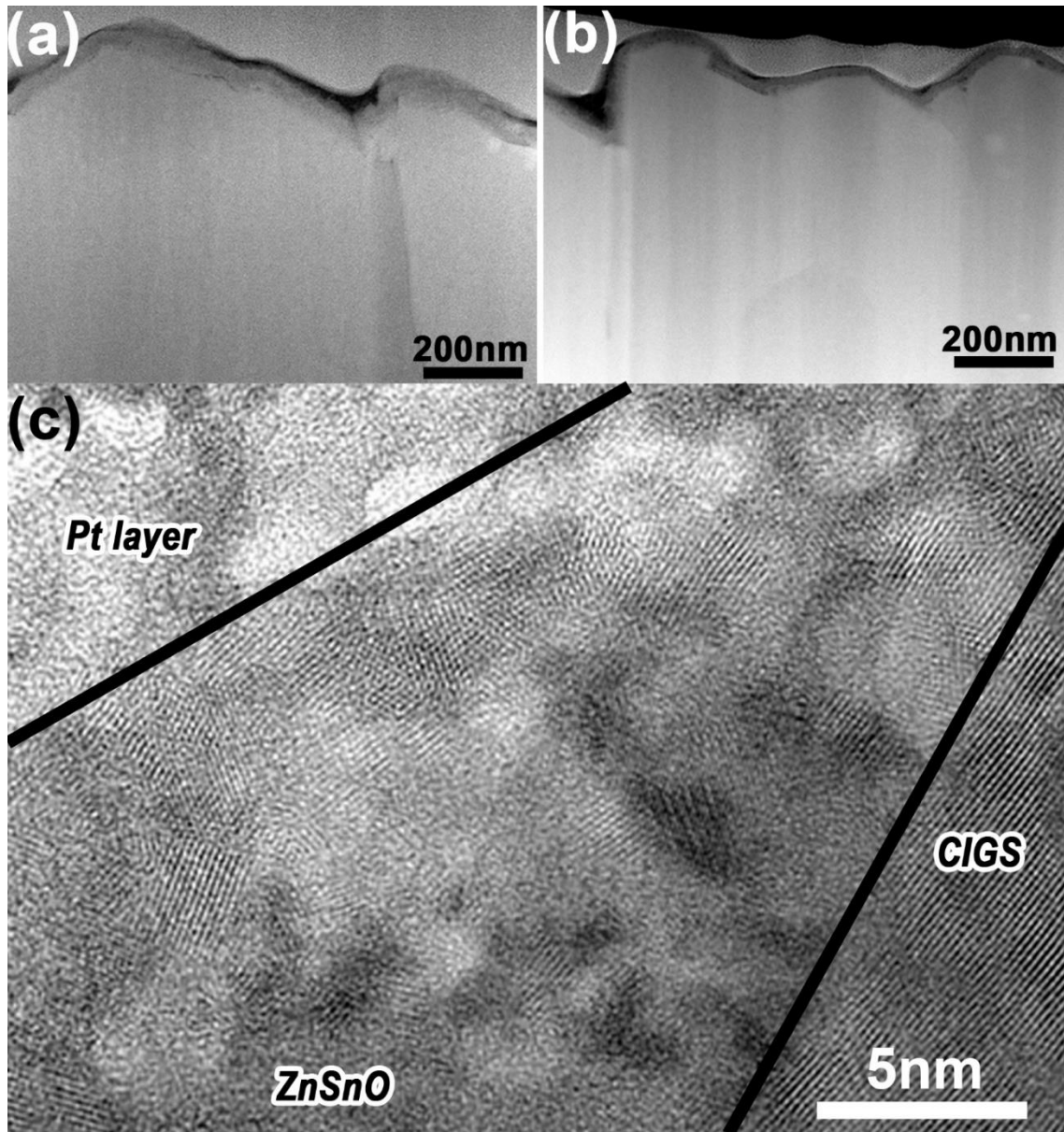


Figure 3: HAADF images of (a) CdS and (b) ZnSnO layers on CIGS. (c) HRTEM image showing nanodomains present in the ZnSnO layer.

Several elemental mappings were performed in different areas of the ZnSnO layer and a representative map is shown in figure 4. The Se and Cu counts superimpose very well, showing where the CIGS layer is located, whereas the Zn counts are also very well defined and they show the position of the ZnSnO layer. From the several elemental mappings performed in the ZnSnO lamella, no diffusion from and/or to the buffer layer was detected. We also performed an EDS linescan, shown in figure 4 e). Since both the EDS mapping and EDS linescan are lengthy measurements, we analysed two different regions to rule out eventual beam damage. The EDS linescan confirms that the CIGS/ZnSnO interface is well defined. There is a superimposition of the CIGS elements with the elements of the ZnSnO layer of  $\sim 10$  nm which is on the

same order of magnitude as the resolution of the EDS signal thus, we cannot rule out some interdiffusion on that scale. The observed superimposition can also be related with interface roughness of the layers located behind the observable region due to the thickness of the lamella. With regards to the CdS sample, the diffusion of elements at the interface is an identified and reported condition in the literature [19-24]. A detailed analysis of that interface is troublesome and quite complex and has been the main topic of several publications with different interpretations and thus is out of the scope of this paper.

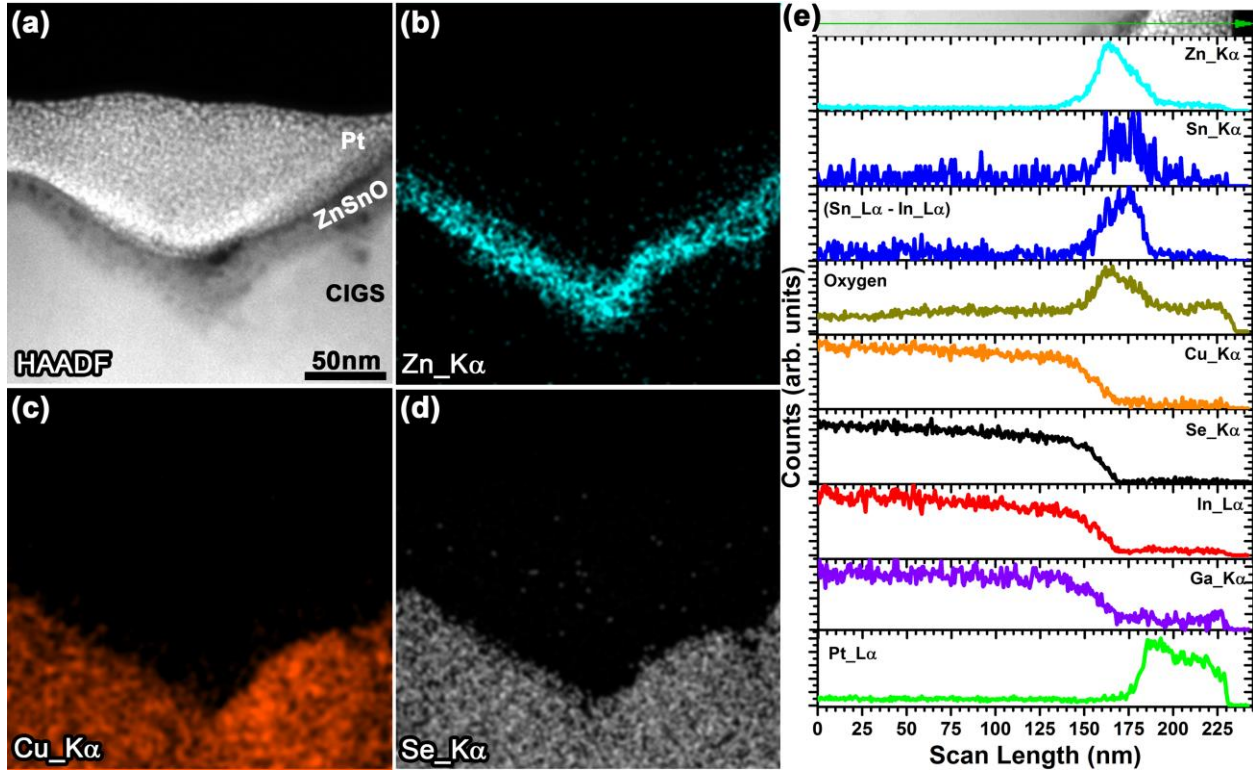


Figure 4: (a) HAADF image and EDS mapping of the ZnSnO sample, showing the elemental mapping for (b) Zn-K $\alpha$ , (c) Cu-K $\alpha$ , and (d) Se-K $\alpha$ , respectively. (e) Depicts an EDS linescan.

### 3.2 Electrical Analysis: J-V and C-V

In Figure 5 representative J-V curves and EQE curves are shown. Table 1 summarizes the data as averages for 12 cells with the corresponding standard deviation values. The results are in accordance with our previous studies that show that the ZnSnO devices can perform as well as, or even outperform, CdS devices [6]. The average values of efficiency show that the ZnSnO devices have a 0.2 % higher efficiency. The improved efficiency of the ZnSnO devices over the CdS ones is due to a higher value of  $J_{sc}$ . In the former, the higher energy EQE behaviour for the side of lower wavelengths, is due to the higher ZnSnO bandgap energy than the corresponding value for the CdS. ZnSnO with a Sn to Zn ratio of 0.2 should have a bandgap energy close to 3.5 eV whereas CdS has a bandgap energy of 2.4 eV [25, 26]. In this study, the  $J_{sc}$  difference between the two devices is in average  $1.1 \text{ mA}\cdot\text{cm}^{-2}$ , nevertheless this value can be as high as  $2 \text{ mA}\cdot\text{cm}^{-2}$  in devices where an AR coating is used [8]. The similarity of the low energy side of the EQE curve confirms that the CIGS absorber layers are indeed equivalent for both samples. In spite of the higher  $J_{sc}$  value of the ZnSnO devices, the measurements also show that they slightly underperform the CdS devices in terms of  $V_{oc}$  and FF values. In this particular case, the differences are small, 5 mV for the  $V_{oc}$  and

1.8 % for the FF, but follow the usual trend of Cd-free buffer layers found in the literature and our previous results [4, 25, 26]. In figure 5 (a), we also show the fitted values of series resistance ( $R_s$ ), shunt resistance ( $R_p$ ), ideality factor ( $n$ ), and saturation current ( $J_0$ ). The values show that for the ZnSnO sample, both resistance values are higher than the ones of CdS. This is in accordance with previous results where it has been shown that the ZnSnO layer, even with only 30 nm, is more resistive than the 50 nm layer of CdS [4, 25- 27]. A highly resistive buffer layer improves  $R_p$ , which is positive for cell performance because the number of shunts is reduced, but at the same could degrade  $R_s$ , which downgrades FF. This result indicates that if we could achieve a full conformal coverage with ZnSnO with a thickness lower than 20 nm, there could likely be some gain in terms of  $R_s$  and thus likely higher values of FF. Both samples show an ideality factor close to 2.

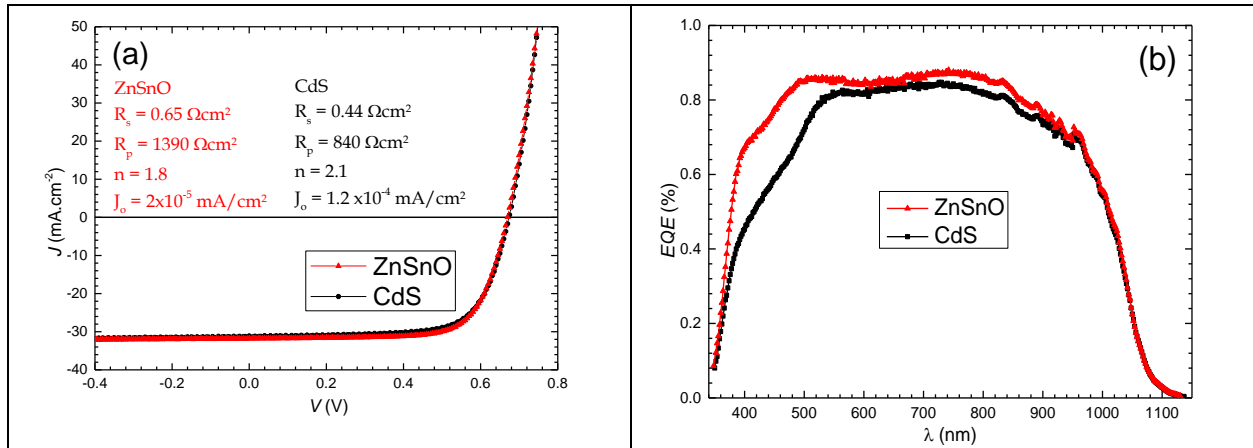


Figure 5: Electrical characterization of CIGS devices with CdS and ZnSnO buffer layer showing representative curves for (a) J-V behaviour and (b) external quantum efficiency.

**Table 1: J-V parameters of devices prepared with CdS and with ZnSnO buffer layers. The values are averages of 12 cells with their respective standard deviations.**

	$J_{sc}$ ( $\text{mA}\cdot\text{cm}^{-2}$ )	$V_{oc}$ (mV)	FF (%)	Efficiency (%)
<b>CdS</b>	$30.62 \pm 0.43$	$671 \pm 3$	$71.1 \pm 0.7$	$14.5 \pm 0.4$
<b>ZnSnO</b>	$31.73 \pm 0.31$	$666 \pm 4$	$69.3 \pm 3.1$	$14.7 \pm 0.7$
<b>Absolute difference (ZnO-CdS)</b>	1.1	-5	-1.8	0.2
<b>Percentage difference (%)</b>	4	-1	-3	1

C-V measurements on both devices were performed and figure 6 summarizes the results. Figure 6 (a) shows that for the CdS sample the capacitance is almost insensitive to frequency, whereas for the ZnSnO, the capacitance is significantly reduced with increasing frequency. Figure 6 (b) shows the Mott-Schottky plot for both devices. The CdS device shows the expected linear behaviour. However, for the ZnSnO device, a very atypical and non-linear behaviour is observed and even a negative value of built-in voltage,  $V_{bi}$ , could be extracted, which has no physical meaning [28, 29]. The depletion region,  $W_{cv}$ , and the net

acceptor concentration,  $N_{cv}$ , are usually extracted from doping profiles, figure 6 (c) [30]. The extraction of  $W_{cv}$  and  $N_{cv}$  is taken at the minimum of the valley [29], which often corresponds to the 0 V condition. In figure 6 (c), the 0 V point is represented by a blue square for each device set of data. While for the CdS device, the minimum of the valley corresponds very closely to the 0 V region, where we extract  $W_{cv}=120$  nm and  $N_{cv} = 5.7 \times 10^{16} \text{ cm}^{-3}$ , for the ZnSnO device, the points are found at different voltages. This analysis shows that for the CdS devices the analysis is straightforward, however, for the ZnSnO devices, several indications point towards an unreliable fit to the simple model: i) a strongly frequency dependent capacitance [31, 32]; ii) a non-linear Mott-Schottky behaviour with negative  $V_{bi}$  values as seen in figure 6 (b); and thereby iii) a doping profile that is very different from the CdS sample [29] as seen in figure 6 (c). There are many possible reasons for the unusual C-V behaviour of the ZnSnO sample, e.g. a high number of traps, high resistance, a frequency variable capacitance among others; and how the solar cell performance would be affected is, at this point, unknown.

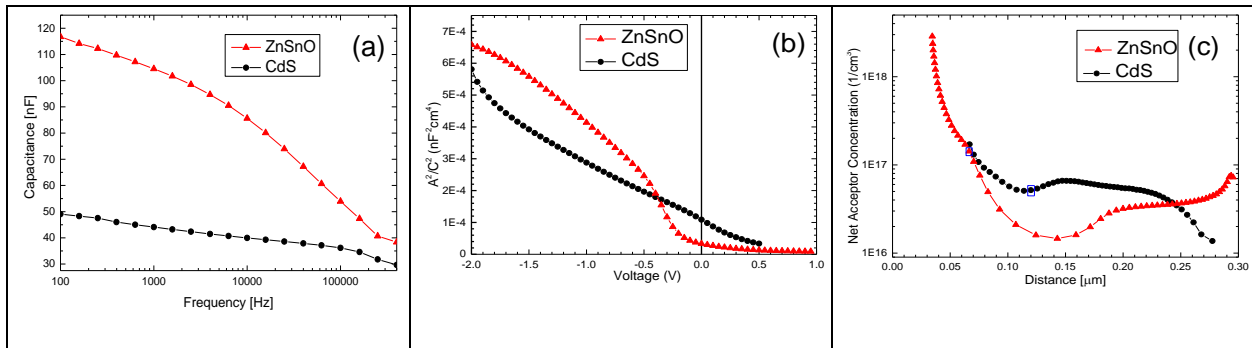


Figure 6: (a) Capacitance versus frequency; (b) Mott-Schottky plot, and (c) doping profiles. In (c) the two blue squares correspond to the 0 V condition.

### 3.3 Kelvin probe force microscopy, surface photovoltage, and photoluminescence

Figure 7 shows the topography and CPD images of the CIGS samples with CdS and ZnSnO buffer layers. Histograms of the distribution of the CPD values measured in the dark (black) and under illumination (red) are also shown. Average values of 10 measurements for each sample are summarized in Table 2. The CPD in the dark of the ZnSnO sample is  $\sim 60$  mV lower than that of the CdS sample. Since the same tip was used for all measurements, a direct comparison between the CPD values is possible. The SPV values for the two samples show a slight difference; the SPV of the CIGS/CdS sample is  $\sim$

10 % higher than that of the CIGS/ZnSnO sample. The SPV is related to the  $V_{oc}$  of the solar cell [17], however a quantitative comparison is not possible here since the SPV was measured for the CIGS/buffer junction, while the  $V_{oc}$  is measured on the full solar cell (absorber, buffer, window). Nevertheless, and even if small, the CdS buffer layer results in a higher voltage in both cases, SPV and  $V_{oc}$ .

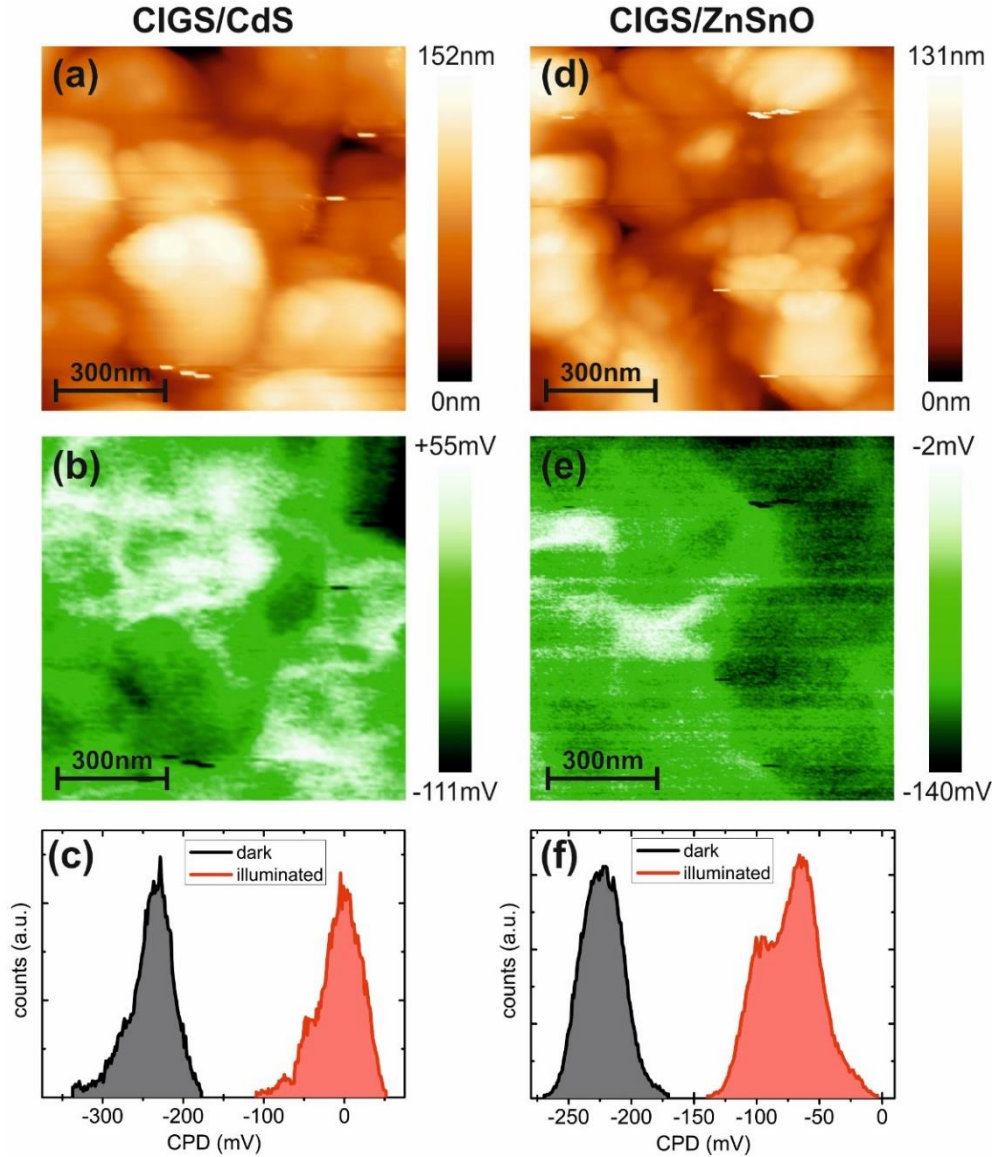


Figure 7: KPFM measurements (a)-(c) on the CIGS/CdS sample and (d)-(f) on CIGS/ZnSnO sample. The topography is shown in (a) and (d), the CPD image in illuminated conditions in (b) and (e). Histograms of the CPD distribution measured in the dark and under illumination are shown in (c) and (f) for CIGS/CdS and CIGS/ZnSnO, respectively.

**Table 2: Average values for  $CPD_{\text{dark}}$  and SPV determined from 10 KPFM measurements taken in 5 different locations for each samples. The standard deviation is also given in both cases.**

	$CPD_{\text{dark}}$ (mV)	SPV (mV)
CIGS/CdS	$-260 \pm 50$	$+183 \pm 55$
CIGS/ZnSnO	$-200 \pm 35$	$+164 \pm 73$

Normalized PL spectra of CdS and ZnSnO are presented in figure 8 (a). For both samples, the emission corresponds to a broad band in the range  $\sim 0.95$ - $1.2$  eV and with a maximum of intensity at  $\sim 1.09$  eV. The emission measured for the CdS sample is slightly blueshifted in comparison to the emission from the ZnSnO sample. The shape of the bands reveal some asymmetry, which is higher for the CdS sample, and is characteristic of electronic transitions occurring in highly doped and strongly compensated semiconductors [33-37]. According to this theory, the asymmetric character of the emission is more evident as the compensation level increases [38-40], which suggests a higher density of ionized defects in the CIGS layer of the CdS sample and/or at the interface with the buffer layer. In order to confirm a larger effect of the fluctuating potentials in the CdS sample, the excitation power dependency on the PL was investigated. Figure 8 (c) shows the obtained dependencies for the peak energy in both samples. The increase of the excitation power, results in a blueshift of 13.5 and 10.5 meV/decade for the CdS and the ZnSnO samples, respectively. Such high shift values are typical of highly doped and compensated semiconductors and confirm the existence of electrostatic fluctuating potentials [38, 41]. Low values of excitation power favour populating of deeper tail states, while the shallower states are just populated for the higher excitation power values. This change from deeper to shallower tail states is reflected in a significant blueshift of the emission. The higher blueshift as well as the higher asymmetry of the emission, figure 8 (a), observed for the CdS sample, suggests a stronger influence of fluctuating potentials in the PL emission of that sample.

For an excitation wavelength of 514.4 nm, most of the volume probed by the PL is in the CIGS layer. To be certain that the CdS layer is not influencing the measurements by absorbing some of the 514.4 nm light, we performed measurements using an excitation laser of 632.8 nm and the spectra were extremely similar. Such observation, that the PL emission using different excitation wavelengths does not differ much, and that CdS does not absorb enough light to influence the emission is in accordance with the literature [42]. The strongest influence of the fluctuations on the PL emission is observed for the CdS sample. In order to obtain an additional confirmation of this behaviour, the CdS buffer was removed by wet etching and we performed PL measurements. Figure 8 (b) shows the measurements before and after removing the CdS layer and the measurements after removing the CdS show an emission with a redshift and with a less asymmetric shape than prior to removing the CdS layer. We note that the behaviour of the PL emission after removing the CdS layer is similar to that observed for the ZnSnO sample. Additionally, the excitation power dependence was investigated and the blueshift decreased from 13.5 to 11.7 meV/decade (see inset in figure 8 (c)). This value is closer to the ZnSnO value. These results give an additional evidence for a higher influence of an increase of the fluctuating potentials in the CIGS layer of the CdS sample.

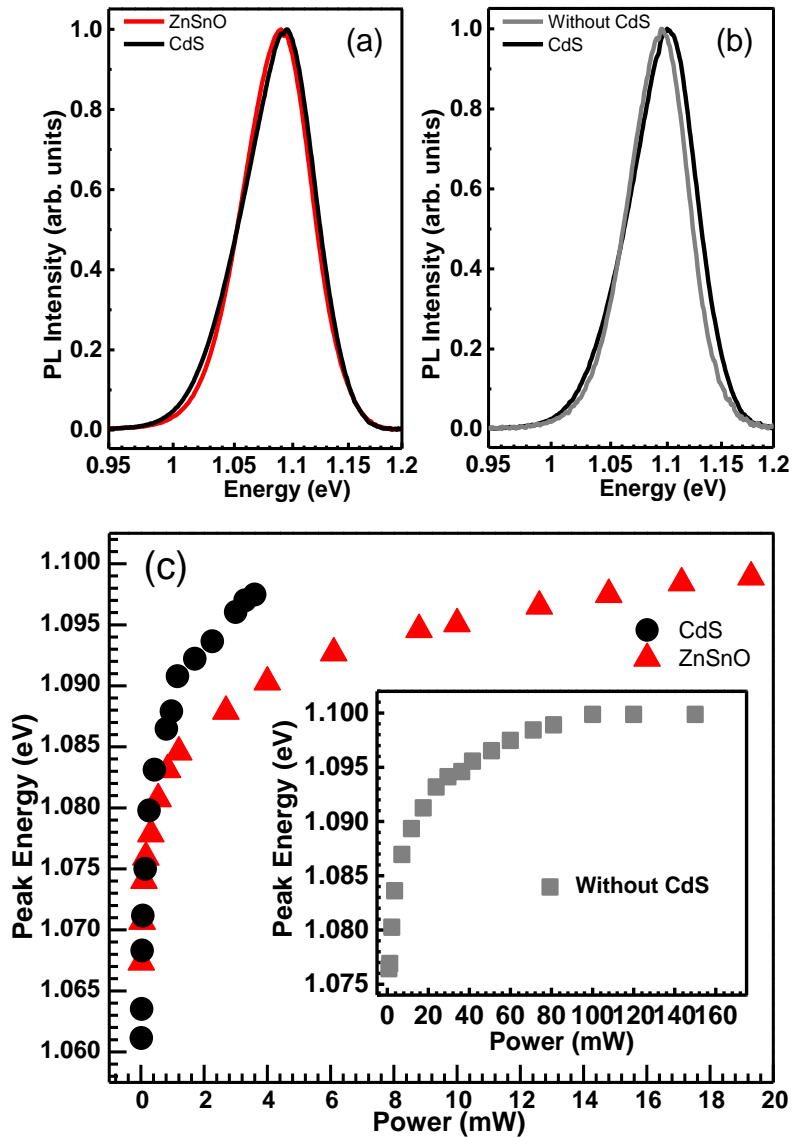


Figure 8. (a) Normalized PL spectra of CdS and ZnSnO samples measured at 5 K and with an excitation power of  $\sim 3.6$  mW. (b) Comparison of the normalized PL spectra of the CdS sample before and after the removal of the CdS buffer layer, measured with an excitation power of 36 mW. (c) Dependence on the excitation power of the peak energy of the broad and asymmetric band for the CdS and ZnSnO samples. The inset shows the same dependence for the CdS sample after the removal of the CdS layer.

#### 4 Discussion of results

In this study we changed only the buffer layer in all of the solar cell processing so that the observed differences are coming from the buffer layer, or from the processing steps of the buffer layer itself. For the transparent conductive oxide and the grids, both devices were processed together and we gave special attention in confirming the similarities of the CIGS absorber layer, since this is the most complex layer to be prepared. From the EQE analysis, we can safely conclude that the CIGS absorbers for each device are

very similar, as expected. This fact confirms that our design of experiment was successful and that differences seen in this study should come from the buffer layer or from its processing.

From the J-V analysis we extracted  $A$  and  $J_0$  for both devices. The higher  $J_0$  value of the CdS devices, compared with the ZnSnO devices, is indicative of higher recombination for that device. Both devices show an ideality factor close to 2 (however, slightly higher for the CdS sample), indicating that both are being limited either by recombination in the space-charge-region or by interface recombination so we can exclude that recombination in the quasi-neutral region is the dominant loss mechanism [43]. In a previous publication with devices similar to the ones presented in this work we studied  $V_{oc}$  as function of temperature and we concluded that for CdS and ZnSnO based devices, interface recombination should not be a limiting factor due to the activation energy of such process to be very close to the absorber band gap energy [44]. Due to the similarity of the solar cell performance it is safe to say that both devices are being limited by the same type of recombination and we can tentatively say that the limitation it is likely to be recombination in the space-charge-region.

The TEM analysis showed that the interface of the CIGS/ZnSnO sample was uniform and within its accuracy no diffusion of elements was detected. For the CdS buffer layers, several diffusion processes have been discussed in the literature, like for instance Cd diffusing into the surface of the CIGS [23] and Cu-depletion of the same surface [22] making it a more complex interface than the CIGS/ZnSnO one. The exact constituent of the CIGS/CdS interface is controversial but in general it is agreed that it is beneficial [20-22, 24, 45] and even it has been debated as the main cause why Cd-free buffer layers have not achieved similar performance as CdS based ones [4,45]. Interfaces affected by intermixing of elements should have a higher number of active defects that potentially participate in the creation of additional fluctuating potentials. Thus, the explanation for the increased effect of fluctuating potentials in the CIGS/CdS sample might be due to the inter-diffusion of atomic species that occurs during the deposition of the CdS layer. This is a strong evidence since after the HCl etch, the influence of the fluctuating potentials on the PL emission lowers and resembles the ZnSnO one. For the PL measurements, the excitation wavelength used ensures that the signal that is seen is mostly from the CIGS layer and the differences seen in the fluctuating potentials between the two samples can be related to effects that include passivation of the surface, modifications to the grain boundaries or diffusion of alien atomic species into the CIGS. The study of fluctuating potentials is quite relevant since this effect has been identified as an important limitation of high-performing CIGS thin film solar cells [45-49]. Thus, the conjugation of J-V, PL, and TEM suggest that CIGS/ZnSnO should have a lower number of ionized defects at the interface than CIGS/CdS. However, this lower number of interface defects is not translated to higher SPV or  $V_{oc}$  values in the CIGS/ZnSnO devices. We attribute this effect to the fact that the main limitation of these solar cells is not interface recombination. Furthermore, the C-V measurements showed that the capacitive behaviour of the ZnSnO cells is quite different from the CdS ones hinting to other electronic differences. A lower number of interface defects that translated into a lower interface recombination rate has also been observed for another Cd-free buffer layer, namely Zn(O,S) [50]. In that study, industrial absorbers from Solar Frontier were processed with a buffer layer consisting of Zn(O,S) and the devices showed a lower interface recombination than devices with a buffer layer of CdS and that resulted in higher values of both  $V_{oc}$  and FF compared with reference CdS devices. However, we note that in the case of [50], the transparent conductive oxide, MOCVD-ZnO:B, is very different from the one used in this work, sputtered-ZnO:Al. Several studies have optimized the CIGS/ZnSnO band alignment to have a positive spike in the order of 0.1 eV [25, 51] but the ZnSnO/window layer has not been optimized. Moreover, it has been pointed out

by Scheer et al. that the conduction band alignment between the buffer layer and the window layer can lead to lower  $V_{oc}$  and FF values [52]. Thus, our observations that the CIGS/ZnSnO interface has a lower number of defects is not contradictory with the possibility of a lower  $V_{oc}$  compared with the CdS sample for two reasons: 1) the alignment between the buffer layer and the window layer can affect  $V_{oc}$  and FF values and has not yet been optimized; 2) the cells are not dominated by interface recombination, so small changes to the interface will not cause significant changes to the cell performance. Due to the lower SPV values of the ZnSnO, we favour the latter explanation since modifications to the bulk of the CIGS can happen during the very different processing conditions of the two buffer layers. During the ALD deposition the absorbers are exposed to 120 °C and several precursor vapours while for the CBD the absorbers are exposed to only 60 °C and liquid solutions that are known to change the composition of the surface and to lower the amount of Na inside the absorber's bulk. Further analysis capable of probing elemental diffusion at parts per billion, e.g. SIMS, would be necessary to fully understand the differences between the samples. Solar cells with Cd-free buffer layers can already attain high values of  $V_{oc}$  and FF [53-55], but further optimizations of the ZnSnO devices are still lacking. Our observation of a 60 mV difference in the CPD between CdS and ZnSnO, together with other characterization techniques, could help to determine absolute values for the work function and electron affinity for ZnSnO. These values for a broad range of compositions are still required since an optimization on the interface buffer layer/window layer must also be considered [56, 57]. The results presented in this paper are also important to design improved strategies for surface passivation of the CIGS/CdS interface [58-64].

## 5 Conclusions

In this study, we fabricated solar cells where all the solar cell layers were the same with the exception of the buffer layer. In one set, CBD-deposited CdS layer was used, whereas in the second set, ALD-deposited ZnSnO was used. CIGS was prepared using a co-evaporation in-line pilot tool that deposits 12.5x12.5 cm<sup>2</sup> substrates with deposition time of 20 minutes. This tool allowed us to prepare solar cells where the only difference between them was the buffer layer. We confirmed that ZnSnO, a non-toxic compound deposited by a vacuum method - ALD, can provide devices with performances very close to CdS. We observed the general trend that Cd-free buffer layers usually provide solar cells with the same efficiency value as Cd-containing ones, higher values of  $J_{sc}$  and with lower values of FF and  $V_{oc}$ , even though the differences observed here are small. The lower  $V_{oc}$  value of the ZnSnO sample, compared with the CdS sample, is in agreement with its lower SPV value. We identified that C-V measurements of ZnSnO-based devices could not be fitted with the simple standard models and in order to take conclusive interpretations, one needs to have other non-destructive measurement techniques capable of probing the depletion region and carrier concentration. The measurements performed in this work tend to indicate that the CIGS/CdS samples have an increased effect of fluctuating potentials of the CIGS layer. Such effect is also present, but to a lower extent, in the CIGS/ZnSnO sample. The lower effect of fluctuating potentials could be related with the non-observable diffusion of elements at the CIGS/ZnSnO interface, contrary to what is reported in the literature for a CIGS/CdS interface. In spite of the fact that the CIGS/ZnSnO interface appears to show a smaller number of defects than the one of CIGS/CdS, it has lower SPV and lower FF values. We correlate this difference to the fact that the devices should not be limited by interface recombination and thus small changes to this parameter will not cause significant changes in the solar cell performance.

## Acknowledgments

P.M.P. Salomé acknowledges financial support from EU through the FP7 Marie Curie IEF 2012 Action No.327367. The authors acknowledge the Swedish Energy Agency (Grant no. 2012-004591), Sweden's innovation agency VINNOVA (Grantno.2013-02199) and STandUP for the financial support. The authors would like to acknowledge the CAPES (CAPES-INL 04/14), CNPq and FAPEMIG funding agencies for the financial support. The projects RECI/FIS-NAN/0183/2012 (COMPETE: FCOMP-01-0124-FEDER-027494) and UID/CTM/50025/2013 from the Fundação para a Ciência e a Tecnologia (Portugal) are also acknowledged.

## References

- [1] R. Kamada, T. Yagioka, S. Adachi, A. Handa, K. Fai Tai, T. Kato, and H. Sugimoto, "New World Record Cu(In,Ga)(Se,S)<sub>2</sub> Thin Film Solar Cell Efficiency Beyond 22%" in 43rd IEEE Photovoltaic Specialists Conference, # 355 (available at <http://www.pvsc-proceedings.org/>) (2016).
- [2] Adrian Chirila, Patrick Reinhard, Fabian Pianezzi, Patrick Bloesch, Alexander R. Uhl, Carolin Fella, Lukas Kranz, Debora Keller, Christina Gretener, Harald Hagendorfer, Dominik Jaeger, Rolf Erni, Shiro Nishiwaki, Stephan Buecheler and Ayodhya N. Tiwari, Potassium-induced surface modification of Cu(In,Ga)Se<sub>2</sub> thin films for high-efficiency solar cells, *Nature Materials*, 12, 1107–1111 (2013).
- [3] Patrick Reinhard, Fabian Pianezzi, Benjamin Bissig, Adrian Chirila, Patrick Blösch, Shiro Nishiwaki, Stephan Buecheler, and Ayodhya N. Tiwari, Cu(In,Ga)Se<sub>2</sub> Thin-Film Solar Cells and Modules— A Boost in Efficiency Due to Potassium, *IEEE JOURNAL OF PHOTOVOLTAICS*, VOL. 5, NO. 2, MARCH 2015.
- [4] N. Naghavi, D. Abou-Ras, N. Allsop, N. Barreau, S. Bücheler, A. Ennaoui, C.-H. Fischer, C. Guillen, D. Hariskos, J. Herrero, R. Klenk, K. Kushiya, D. Lincot, R. Menner, T. Nakada, C. Platzer-Björkman, S. Spiering, A.N. Tiwari and T. Törndahl, Buffer layers and transparent conducting oxides for chalcopyrite Cu(In,Ga)(S,Se)<sub>2</sub> based thin film photovoltaics: present status and current *PROGRESS IN PHOTOVOLTAICS: RESEARCH AND APPLICATIONS*, 2010; 18:411–433.
- [5] Theresa Magorian Friedlmeier, Philip Jackson, Andreas Bauer, Dimitrios Hariskos, Oliver Kiowski, Roland Wuerz, and Michael Powalla, Improved Photocurrent in Cu(In,Ga)Se<sub>2</sub> Solar Cells: From 20.8% to 21.7% Efficiency with CdS Buffer and 21.0% Cd-Free, *IEEE JOURNAL OF PHOTOVOLTAICS*, VOL. 5, NO. 5, SEPTEMBER 2015.
- [6] J. Lindahl, J. T. Wätjen, A. Hultqvist, T. Ericson, M. Edoff, T. Törndahl, The effect of Zn<sub>1-x</sub>S<sub>x</sub>O<sub>y</sub> buffer layer thickness in 18.0% efficient Cd-free Cu(In,Ga)Se<sub>2</sub> solar cells, *Prog. Photovolt: Res. Appl.* 2013; 21:1588–1597.
- [7] Jan Keller, Johan Lindahl, Marika Edoff, Lars Stolt, Tobias Törndahl, Potential gain in photocurrent generation for Cu(In,Ga)Se<sub>2</sub> solar cells by using In<sub>2</sub>O<sub>3</sub> as a transparent conductive oxide layer, *Prog. Photovolt: Res. Appl.* (2015) DOI: 10.1002/pip.2655.
- [8] Johan Lindahl, Uwe Zimmermann, Piotr Szaniawski, Tobias Törndahl, Adam Hultqvist, Pedro Salomé, Charlotte Platzer-Björkman, and Marika Edoff, In-line Cu(In,Ga)Se<sub>2</sub> Co-evaporation for High Efficiency Solar Cells and Modules, *IEEE JOURNAL OF PHOTOVOLTAICS*, VOL. 3, NO. 3, JULY 2013.

- [9] P.M.P. Salomé, A. Hultqvist, V. Fjällström, M. Edoff, B.G. Aitken, K. Zhang, K. Fuller and C. Kosik Williams, Incorporation of Na in Cu(In,Ga)Se<sub>2</sub> thin film solar cells: a statistical comparison between Na from soda lime glass and from a precursor layer of NaF, IEEE Journal of Photovoltaics, VOL. 4, NO. 6, NOVEMBER 2014.
- [10] P.M.P. Salomé, V. Fjällström, A. Hultqvist, P. Szaniawski, U. Zimmermann and M. Edoff, The effect of Mo back contact ageing on CIGS thin film solar cells, Progress in Photovoltaics: Research and Applications, Volume 22, Issue 1, pages 83–89, January 2014.
- [11] P.M.P. Salomé, V. Fjällström, P. Szaniawski, J.P. Leitão, A. Hultqvist, P.A. Fernandes, J. P. Teixeira, B. P. Falcão, U. Zimmermann, A.F. da Cunha and M. Edoff, A comparison between thin film solar cells made from co-evaporated CuIn<sub>1-x</sub>Ga<sub>x</sub>Se<sub>2</sub> using a one-stage process versus a three-stage process, Progress in Photovoltaics: Research and Applications, 2015; 23:470–478.
- [12] P.M.P. Salomé, A. Hultqvist, V. Fjällström, M. Edoff, B. Aitken, K. Vaidyanathan, K. Zhang, K. Fuller and C. Kosik Williams, Cu(In,Ga)Se<sub>2</sub> solar cells with varying Na content prepared on nominally alkali-free glass substrates, IEEE Journal of Photovoltaics, VOL. 3, NO. 2, APRIL 2013.
- [13] Wyatt K. Metzger, Ingrid L. Repins, and Miguel A. Contreras, Long lifetimes in high-efficiency Cu(In,Ga)Se<sub>2</sub> solar cells, Applied Physics Letters 93, 022110 (2008).
- [14] W.K. Metzger, I.L. Repins, M. Romero, P. Dippo, M. Contreras, R. Noufi, D. Levi, Recombination kinetics and stability in polycrystalline Cu(In,Ga)Se<sub>2</sub> solar cells, Thin Solid Films 517 (2009) 2360–2364.
- [15] Steven S. Hegedus and William N. Shafarman, Thin-Film Solar Cells: Device Measurements and Analysis, Prog. Photovolt: Res. Appl. 2004;12:155–176 (DOI: 10.1002/pip.518).
- [16] Bals S, Tirry W, Geurts R, Yang Z and Schryvers D, High-quality sample preparation by low kV FIB thinning for analytical TEM measurements, Microsc Microanal. 2007 Apr;13(2):80-6.
- [17] S. Sadewasser, Surface potential of chalcopyrite films measured by KPFM, phys. stat. sol. (a) 203, No. 11, 2571–2580 (2006) / DOI 10.1002/pssa.200669573.
- [18] P.M.P. Salomé, A. Hultqvist, V. Fjällström, B. Vermang, M. Edoff, B. Aitken, K. Zhang, K. Fuller and C. Kosik Williams, The effect of high growth temperature on Cu(In,Ga)Se<sub>2</sub> thin film solar cells, Solar Energy Materials & Solar Cells 123 (2014) 166–170.
- [19] Yanfa Yan, R. Noufi, K. M. Jones, K. Ramanathan, and M. M. Al-Jassim, B. J. Stanbery, Chemical fluctuation-induced nanodomains in C(In,Ga)Se<sub>2</sub> films, Appl. Phys. Lett. 87, 121904 (2005).
- [20] C. Lei, M. Duch, I. M. Robertson, and A. Rockett, Effects of solution-grown CdS on Cu(In,Ga)Se<sub>2</sub> grain boundaries, J. Appl. Phys. 108, 114908 (2010).
- [21] Bao Lei, William W. Hou, Sheng-Han Li, Wenbing Yang, Choong-Heui Chung, Yang Yang, Cadmium ion soaking treatment for solution processed CuInS<sub>x</sub>Se<sub>2-x</sub> solar cells and its effects on defect properties, Solar Energy Materials & Solar Cells 95 (2011) 2384–2389.
- [22] Dongxiang Liao, and Angus Rockett, Cu depletion at the CuInSe<sub>2</sub> surface, Appl. Phys. Lett., Vol. 82, No. 17, 28 April 2003

- [23] T. Nakada and A. Kunioka, Direct evidence of Cd diffusion into Cu(In,Ga)Se<sub>2</sub> thin films during chemical-bath deposition process of CdS films, *Appl. Phys. Lett.*, Vol. 74, No. 17, 26 April 1999.
- [24] Chun-Sheng Jiang, F. S. Hasoon, H. R. Moutinho, H. A. Al-Thani, M. J. Romero and M. M. Al-Jassim, Direct evidence of a buried homojunction in Cu(In,Ga)Se<sub>2</sub> solar cells *Appl. Phys. Lett.*, Vol. 82, No. 1, 6 January 2003
- [25] Mukes Kapilashrami, Coleman X. Kronawitter, Tobias Torndahl, Johan Lindahl, Adam Hultqvist, Wei-Cheng Wang, Ching-Lin Chang, Samuel S. Mao and Jinghua Guo, Soft X-ray characterization of Zn<sub>1-x</sub>Sn<sub>x</sub>O<sub>y</sub> electronic structure for thin film photovoltaics, *Phys. Chem. Chem. Phys.*, 2012, 14, 10154–10159
- [26] Johan Lindahl, Carl Hägglund, J. Timo Wätjen, Marika Edoff, Tobias Törndahl, The effect of substrate temperature on atomic layer deposited zinc tin oxide, *Thin Solid Films* Volume 586, 1 July 2015, Pages 82–87.
- [27] Adam Hultqvist, Charlotte Platzer-Björkman, Uwe Zimmermann, Marika Edoff and Tobias Törndahl, Growth kinetics, properties, performance, and stability of atomic layer deposition Zn–Sn–O buffer layers for Cu(In,Ga)Se<sub>2</sub> solar cells, *Prog. Photovolt: Res. Appl.* 2012; 20:883–891
- [28] Tobias Eisenbarth, Thomas Unold, Raquel Caballero, Christian A. Kaufmann, and Hans-Werner Schock, Interpretation of admittance, capacitance-voltage, and current-voltage signatures in Cu(In,Ga)Se<sub>2</sub> thin film solar cells, *J. Appl. Phys.* 107, 034509 (2010); doi: 10.1063/1.3277043.
- [29] Michal Cwil, Malgorzata Igalson, Pawel Zabierowski and Susanne Siebentritt, Charge and doping distributions by capacitance profiling in Cu(In,Ga)Se<sub>2</sub> solar cells, *J. Appl. Phys.* 103, 063701 (2008).
- [30] Jennifer T. Heath, J. David Cohen, and William N. Shafarman, Bulk and metastable defects in CuIn<sub>1-x</sub>Ga<sub>x</sub>Se<sub>2</sub> thin films using drive-level capacitance profiling, *J. Appl. Phys.*, Vol. 95, No. 3, 1 February 2004.
- [31] W. A. Striffler and C. W. Bates, Jr. Admittance spectroscopy of CuInSe<sub>2</sub>/CdS solar cells prepared by chemical spray pyrolysis, *J. Appl. Phys.* 71, 4358 (1992).
- [32] Lawrence V. Hmurcik and Raymond A. Serway, Frequency dependent capacitance studies of the CdS/Cu<sub>2</sub>S thin-film solar cell, *Journal of Applied Physics* 53, 3830 (1982); doi: 10.1063/1.331127.
- [33] A. P. Levanyuk and V. V. Osipov, *Soviet Phys. Usp.* 24, 187 (1981).
- [34] I. Dirnstorfer, D. M. Hofmann, D. Meister, B. K. Meyer, W. Riedl, and F. Karg, *J. Appl. Phys.* 85, 1423 (1999).
- [35] A. Bauknecht, S. Siebentritt, J. Albert, and M. C. Lux-Steiner, *J. Appl. Phys.* 89, 4391 (2001).
- [36] J. P. Leitão, N. M. Santos, P. A. Fernandes, P. M. P. Salomé, A. F. da Cunha, J. C. González, G. M. Ribeiro, and F. M. Matinaga, *Phys. Rev. B* 84, 024120 (2011).
- [37] M. J. Romero, H. Du, G. Teeter, Y. Yan, and M. M. Al-Jassim, Comparative study of the luminescence and intrinsic point defects in the kesterite Cu<sub>2</sub>ZnSnS<sub>4</sub> and chalcopyrite Cu(In,Ga)Se<sub>2</sub> thin films used in photovoltaic applications, *Phys. Rev. B* 84, 165324 (2011).

- [38] Phil Won Yu, Excitationdependent emission in Mg, Be, Cd, and Znimplanted GaAs, *J. Appl. Phys.* 48, 5043 (1977); doi: 10.1063/1.323631.
- [39] Phil Won Yu, Radiative recombination in melt grown and Cd implanted  $\text{CuInSe}_2$ , *J. Appl. Phys.* 47, 677 (1976); doi: 10.1063/1.322633.
- [40] J. P. Teixeira, R. A. Sousa, M. G. Sousa, A. F. da Cunha, P. A. Fernandes, P. M. P. Salomé, J. C. González, and J. P. Leitão, Comparison of fluctuating potentials and DAP transitions in a Cu-poor  $\text{Cu}_2\text{ZnSnS}_4$  based solar cell, *Applied Physics Letters*, 105, 163901 (2014).
- [41] J. P. Teixeira, R. A. Sousa, M. G. Sousa, A. F. da Cunha, P. A. Fernandes, P. M. P. Salomé and J. P. Leitão, Radiative transitions in highly doped and compensated chalcopyrites and kesterites: The case of  $\text{Cu}_2\text{ZnSnS}_4$ , *Physical Review B* 90 (23), 235202 (2014).
- [42] L. Lombez, M. Soro, A. Delamarre, N. Naghavi, N. Barreau, D. Lincot, and J.-F. Guillemoles, Revisiting the interpretation of biased luminescence: Effects on  $\text{Cu}(\text{In,Ga})\text{Se}_2$  photovoltaic heterostructures, *JOURNAL OF APPLIED PHYSICS* 116, 064504 (2014)
- [43] R. Scheer, Towards an electronic model for  $\text{CuIn}_{1-x}\text{Ga}_x\text{Se}_2$  solar cells, *Thin Solid Films* 519 (2011) 7472–7475.
- [44] Johan Lindahl, Jan Keller, Olivier Donzel-Gargand, Piotr Szaniawski, Marika Edoff, Tobias Törndahl, Deposition temperature induced conduction band changes in zinc tin oxide buffer layers for  $\text{Cu}(\text{In,Ga})\text{Se}_2$  solar cells, *Sol. Energy Mater. Sol. Cells*, 144 (2016) 684.
- [45] K. Ramanathan, F.S. Hasoon, S. Smith, D.L. Young, M.A. Contreras, P.K. Johnson, A.O. Pudov, J.R. Sites, Surface treatment of  $\text{Cu}(\text{In,Ga})\text{Se}_2$  thin films and its effect on the photovoltaic properties of solar cells, *Journal of Physics and Chemistry of Solids* 64 (2003) 1495–1498.
- [46] U. Rau and J. H. Werner, Radiative efficiency limits of solar cells with lateral bandgap fluctuations, *Appl. Phys. Lett.* 84, 3735 (2004).
- [47] S. Siebentritt, What limits the efficiency of chalcopyrite solar cells?, *Sol. Energy Mater. Sol. Cells* 95, 1471 (2011).
- [48] T. Gokmen, O. Gunawan, T. K. Todorov, and D. B. Mitzi, Band tailing and efficiency limitation in kesterite solar cells, *Appl. Phys. Lett.* 103, 103506 (2013).
- [49] P. Pistor, D. Greiner, C. A. Kaufmann, S. Brunken, M. Gorgoi, A. Steigert, W. Calvet, I. Lauermann, R. Klenk, T. Unold, and M.C. Lux-Steiner, Experimental indication for band gap widening of chalcopyrite solar cell absorbers after potassium fluoride treatment, *Appl. Phys. Lett.* 105, 063901 (2014).
- [50] Taizo Kobayashi, Zacharie Jehl Li Kao, Takuya Kato, Hiroki Sugimoto and Tokio Nakada, A comparative study of Cd- and Zn-compound buffer layers on  $\text{Cu}(\text{In}_{1-x}\text{Ga}_x)(\text{S}_y\text{Se}_{1-y})_2$  thin film solar cells, *Prog. Photovolt: Res. Appl.* (2015), DOI: 10.1002/pip.2695.
- [51] Takashi Minemoto, Akira Okamoto, Hideyuki Takakura, Sputtered ZnO-based buffer layer for band offset control in  $\text{Cu}(\text{In,Ga})\text{Se}_2$  solar cells, *Thin Solid Films* 519 (2011) 7568–7571.

- [52] R. Scheer, H. Wilhelm, Efficiency limitations of chalcopyrite and kesterite solar cells, Photovoltaic Specialists Conference (PVSC), 2011 37th IEEE, 002500 - 002505
- [53] Junggyu Nam, Yoonmook Kang, Dongho Lee, JungYup Yang, Young-Su Kim, Chan B. Mo, Sungchan Park and Dongseop Kim, Achievement of 17.9% efficiency in 30×30cm<sup>2</sup> Cu(In,Ga)(Se,S)<sub>2</sub> solar cell sub-module by sulfurization after selenization with Cd-free buffer, Prog. Photovolt: Res. Appl. (2015) DOI: 10.1002/pip.2653.
- [54] Suncheul Kim, Chang-Soo Lee, Seungtae Kim, R. B. V. Chalapathy, Essam A. Al-Ammar and Byung Tae Ahn, Understanding the light soaking effect of ZnMgO buffer in CIGS solar cells, Phys. Chem. Chem. Phys., 2015, 17, 19222.
- [55] Christian Schubbert, Patrick Eraerds, Michael Richter, Jürgen Parisi, Ingo Riedel, Thomas Dalibor, and Jörg Palm, Anomalous temperature dependence of the open-circuit voltage of In<sub>x</sub>S<sub>y</sub>-buffered Cu(In,Ga)(Se,S)<sub>2</sub> solar cells simulated in broad temperature range, Phys. Status Solidi A, 1–8 (2015) / DOI 10.1002/pssa.201532534.
- [56] Timo Jäger, Yaroslav E. Romanyuk, Benjamin Bissig, Fabian Pianezzi, Shiro Nishiwaki, Patrick Reinhard, Jérôme Steinhauser, Johannes Schwenk, and Ayodhya N. Tiwari, Improved open-circuit voltage in Cu(In,Ga)Se<sub>2</sub> solar cells with high work function transparent electrodes, J. Appl. Phys. 117, 225303 (2015).
- [57] Negar Naghavi, Solange Temgoua, Thibaud Hildebrandt, Jean François Guillemoles and Daniel Lincot, Impact of oxygen concentration during the deposition of window layers on lowering the metastability effects in Cu(In,Ga)Se<sub>2</sub>/CBD Zn(S,O) based solar cell, Prog. Photovolt: Res. Appl. (2015), DOI: 10.1002/pip.2626.
- [58] P. Jackson, D. Hariskos, R. Wuerz, O. Kiowski, A. Bauer, T. M. Friedlmeier, and M. Powalla, Properties of Cu(In,Ga)Se<sub>2</sub> solar cells with new record efficiencies up to 21.7%, Phys. Status Solidi - Rapid Res. Lett. 9, 28 (2015).
- [59] F. Pianezzi, P. Reinhard, A. Chirilă, B. Bissig, S. Nishiwaki, S. Buecheler, and A. N. Tiwari, Unveiling the effects of post-deposition treatment with different alkaline elements on the electronic properties of CIGS thin film solar cells, Phys. Chem. Chem. Phys. 16, 8843 (2014).
- [60] A. Laemmle, R. Wuerz, and M. Powalla, Efficiency enhancement of Cu(In,Ga)Se<sub>2</sub> thin-film solar cells by a post-deposition treatment with potassium fluoride, Phys. Status Solidi - Rapid Res. Lett. 7, 631 (2013).
- [61] Bart Vermang, Viktor Fjällström, Jonas Pettersson, Pedro Salomé, and Marika Edoff, Development of Rear Surface Passivated Cu(In,Ga)Se<sub>2</sub>, Thin Film Solar Cells with Nano-Sized Local Rear Point Contacts, Solar Energy Materials & Solar Cells 117 (2013) 505–511.
- [62] Bart Vermang, Jörn Timo Wätjen, Christopher Frisk, Viktor Fjällström, Fredrik Rostvall, Marika Edoff, Pedro Salomé, Jérôme Borme, Nicoleta Nicoara, Sascha Sadewasser, Introduction of Si PERC rear contacting design to boost efficiency of Cu(In,Ga)Se<sub>2</sub> solar cells, IEEE Journal of Photovoltaics, VOL. 4, NO. 6, NOVEMBER 2014.
- [63] A. Hultqvist, J. V. Li, D. Kuciauskas, P. Dippo, M. A. Contreras, D. H. Levi, and S. F. Bent, Reducing interface recombination for Cu(In,Ga)Se<sub>2</sub> by atomic layer deposited buffer layers, Appl. Phys. Lett. 107, 033906 (2015).

[64] Shi Luo, Carissa Eisler, Tsun-Hsin Wong, Hai Xiao, Chuan-En Lin, Tsung-Ta Wu, Chang-Hong Shen, Jia-Min Shieh, Chuang-Chuang Tsai, Chee-Wee Liu, Harry A. Atwater, William A. Goddard III, Jiun-Haw Lee, Julia R. Greer, Suppression of surface recombination in CuInSe<sub>2</sub> (CIS) thin films via Trioctylphosphine Sulfide (TOP:S) surface passivation, *Acta Materialia* 106 (2016) 171-181.

## List of captions

Figure 1: Representation of the fabrication and design of experiment. In the process of fabricating the solar cell, the only step where the devices were not processed at the same time was the buffer layer deposition.

Figure 2: Elemental depth profile of  $[\text{Ga}]/([\text{Ga}] + [\text{In}])$ ,  $[\text{Cu}]/([\text{Ga}] + [\text{In}])$ , and counts of Na and Mo, measured by GDOES for the studied CIGS samples and with an overall  $[\text{Ga}]/([\text{Ga}] + [\text{In}])$  value of 42 %. The values of  $[\text{Ga}]/([\text{Ga}] + [\text{In}])$ ,  $[\text{Cu}]/([\text{Ga}] + [\text{In}])$  were calibrated using XRF measurements.

Figure 3: HAADF images of (a) CdS and (b) ZnSnO layers on CIGS. (c) HRTEM image showing nanodomains present in the ZnSnO layer.

Figure 4: (a) HAADF image and EDS mapping of the ZnSnO sample, showing) the elemental mapping for (b) Zn-K $\alpha$ , (c) Cu-K $\alpha$ , and (d) Se-K $\alpha$ , respectively.

Figure 5: Electrical characterization of CIGS devices with CdS and ZnSnO buffer layer showing representative curves for (a) J-V behavior and (b) external quantum efficiency.

Figure 6: (a) Capacitance versus frequency; (b) Mott-Schottky plot, and (c) doping profiles. In (c) the two blue squares correspond to the 0 V condition.

Figure 7: KPFM measurements (a)-(c) on the CIGS/CdS sample and (d)-(f) on CIGS/ZnSnO sample. The topography is shown in (a) and (d), the CPD image in illuminated conditions in (b) and (e). Histograms of the CPD distribution measured in the dark and under illumination are shown in (c) and (f) for CIGS/CdS and CIGS/ZnSnO, respectively.

Figure 8. (a) Normalized PL spectra of CdS and ZnSnO samples measured at 5 K and with an excitation power of  $\sim 3.6$  mW. (b) Comparison of the normalized PL spectra of the CdS sample before and after the removal of the CdS buffer layer, measured with an excitation power of 36 mW. (c) Shows the dependence on the excitation power of the peak energy of the broad and asymmetric band for the CdS and ZnSnO samples. The inset shows the same dependence for the CdS sample after the removal of the CdS layer.